International Design Engineering Technical Conferences
Computers and Information in Engineering Conference
IDETC-CIE 2022
August 14–August 17, 2022, St. Louis, MO

IDETC2022-89801

SELF-ALIGNING ROTATIONAL LATCHING MECHANISMS

Gabriel I. Fernandez[†,*], Samuel Gessow[†,*], Justin Quan[*], Dennis Hong[*]

Robotics and Mechanisms Laboratory (RoMeLa), Department of Mechanical and Aerospace Engineering
University of California Los Angeles, Los Angeles, CA, 90024

ABSTRACT

In concurrent work, we introduced a novel robotic package delivery system LIMMS (Latching Intelligent Modular Mobility System). Each of LIMMS' end effectors requires a small, lightweight latching mechanism for pre-manufactured containers such as cardboard boxes. In order to effectively process a high volume of packages, aligning the latching mechanism quickly and reliably becomes critical. Instead of depending on highly accurate controllers for alignment, we propose a novel self-aligning rotational mechanism to increase the system's tolerance to misalignment. The latching design consists of evenly spaced blades that rotate into slots cut into the box. When misaligned, the blades contact the edges of the engagement slots, generating a self-correcting force that passively centers the blades with the slot pattern. This paper introduces a mathematical framework with closed form expressions to quantify error tolerance for for these mechanisms. Through our mathematical and optimization analyses, it is shown that a 2-blade design can tolerate a maximum misalignment: $\sqrt{5} \approx 2.236$ times the radius of the blade tips. Our approach can be generalized for a class of rotational latching mechanisms with any number of blades. Utilizing this theory, a design process is laid out for developing an optimal self-aligning rotational latching mechanism given desired parameters and task constraints. With this methodology, we designed, manufactured, and verified the effectiveness of both 2-blade and 3-blade self-aligning latches in practical experiments.

Keywords: Latch, Design, Mechanisms, Rotating, Self-Correcting, Self-Aligning, Symmetric, Robust, Modular, Robot, Delivery, Logistics, Multi-Modal, Legged, Wheel

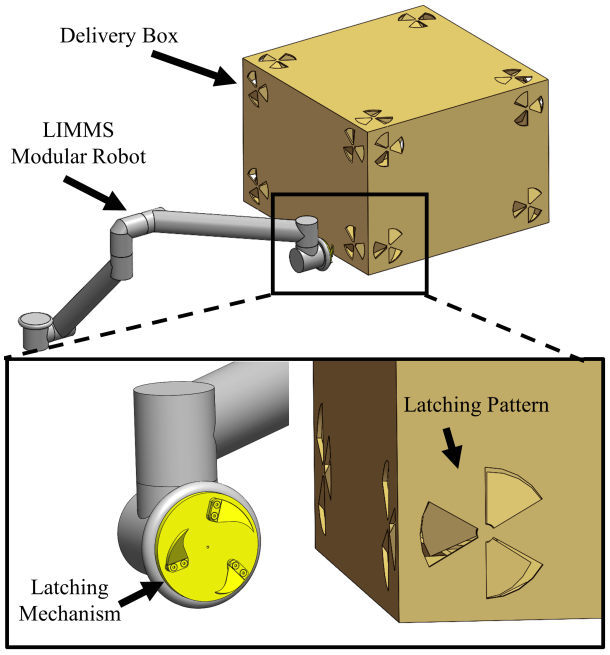

FIGURE 1: LIMMS PLATFORM WITH A 3-BLADE LATCH DESIGN NEXT TO A BOX TO BE DELIVERED WITH MATING HOLES IN THE CARDBOARD TO BE USED AS ANCHOR POINTS.

NOMENCLATURE

$\alpha_1, \alpha_2, \alpha_3$	arc length between intersections, Fig. 6
β_1, β_2	angle from sector edge to line through r', Fig. 6
F_N, μ	normal force and coefficient of friction, Fig. 5
γ	angle of blade tip about (r', θ), Sec. 4
IC	instant center, Fig. 5
l_1, l_2	arc length of unblocked α_1 and α_2, Fig. 6
p	probability of latching success for a position, Sec. 4
ϕ_1	half of the angle blocking the circle, Fig. 6
ϕ_2	angle defined by ϕ_1 and blocking point, Fig. 6
Ψ	misalignment tolerance metric, Sec. 4
r	cutout center to nearest hole edge, Fig. 2
r'	blade assembly center to cutout center, Fig. 5
R	radial length of cutout, Sec. 4
ρ	blade assembly center to blade tips, Fig. 2
τ	torque applied to blade assembly center, Fig. 4
θ	angle between r' and sector edge, Fig. 5
V	velocity, Fig. 5
W	blade assembly center to outer limit, Fig. 2
x, y	Cartesian coordinates of r and θ, Sec. 4

Superscripts and Subscripts

$*$	Indicates an optimal parameter
in, out	Refers to inner and outer alignments respectively
$\|$	Separates a functions inputs from given parameters

[†]Joint first authors
[*]Corresponding author: gabriel808@ucla.edu, sgessow@ucla.edu, justinquan@ucla.edu, dennishong@ucla.edu

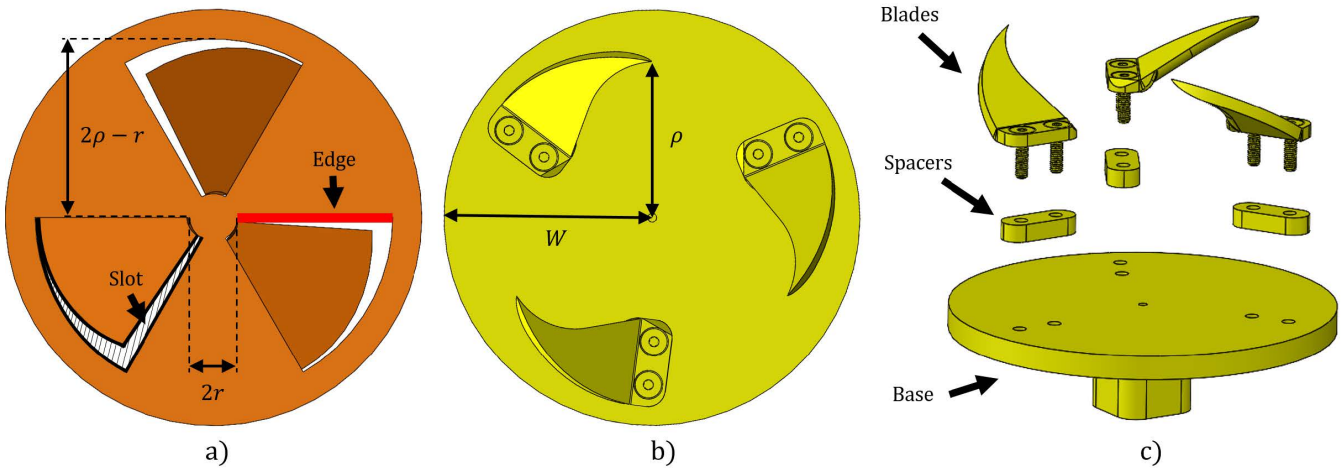

FIGURE 2: A) *LATCHING PATTERN* CUT FROM CARDBOARD WITH RED LINES DENOTING ENGAGEMENT EDGES WHERE THE BLADES CONTACT WHEN FULLY ENGAGED, B) *LATCH* ASSEMBLED CONFIGURATION, AND C) COMPONENTS OF THE LATCH.

1. INTRODUCTION

To solve the last-mile delivery problem, we recently introduced LIMMS (Latching Intelligent Modular Mobility System) [1]. LIMMS is a novel decentralized robotic system that operates without a primary body. A single LIMMS unit resembles an appendage with latching mechanisms on both ends, which can serve as either the end effector or the base, as shown in Fig. 1. After securing one end to a fixed structure, the other end is free to behave like a manipulator or leg. For example, LIMMS can attach itself to anchor points on the surface of a wall to function as a manipulator, or four LIMMS latched to four corners of a box could walk like a quadruped, with the box itself serving as its body. Throughout the delivery process, LIMMS will have to frequently switch between walking and manipulating to process packages, which requires frequent latching and unlatching. Given the massive volume of packages shipped daily and the demand for faster delivery times, it is important to ensure that latching can happen quickly and reliably, or it can become a bottleneck that limits delivery times.

To perform its primary functions, LIMMS must be equipped with a latching mechanism that interfaces seamlessly with both cardboard and wall-mounted anchor points integrated in delivery vehicles. Latching mechanisms for attaching and detaching components have been explored for a wide variety of applications, including tool changers [2], space vessel docking [3], and modular robotics [4, 5]. The latching method varies widely depending on the use case, including passive spring-loaded locks, magnetic locks, and pneumatically actuated locks. In most cases latching mechanisms rely on highly specialized male and female connectors with complex features to assist with alignment such as opposing grip claws [6], floating devices [7], and ball plungers [8].

While these examples offer robust alignment and load support capabilities, LIMMS has several operational restrictions that make these conventional approaches unsuitable. First, the mating surface of the latching mechanism must be very cheap to integrate onto cardboard delivery boxes, since it is assumed that the box will be discarded after use. This means any additions to the box must have a small footprint and low mass to minimize production and delivery costs, respectively. Second, the mechanism should have a small volume and have minimal protruding features with mating surfaces in order to minimize the amount of volume lost in boxes and delivery vehicles. Finally, the mechanism's overall mass should be as small as possible, since excess weight at the LIMMS end effectors will negatively impact its load capacity and walking capabilities.

With these restrictions, the proposed solution is to integrate a female latching pattern on the cardboard delivery package. This involves cutting planar features and folding them out of plane to form flaps into the surface that can assist with alignment, depicted in Fig. 2, 4. This method results in a very low cost latching pattern for disposable cardboard. The male latch will be a lightweight radial design with blades that insert into the engagement slots cut into the cardboard pattern with a twisting motion. This design passively aligns itself as it rotates, using contact forces from the pattern geometry. The simple construction of this latching mechanism results in minimal mass added to the end effector.

Our proposed framework leverages geometry and mechanics to design a self-aligning mechanism with maximum misalignment tolerance, minimizing time spent on alignment during operations. This is achieved by radially symmetric patterns on both end effectors and anchor points.

For our application, the mechanics for self-aligning and its associated misalignment sensitivity for the 2-blade and 3-blade end effector designs are formally derived with closed form expressions. From this, we formulate a metric associated with misalignment tolerance. By choosing a desired tolerance, our mathematical models will calculate optimal design specifications for the latching mechanism and hole pattern. Our methodology is formulated in a general case so it may also be used for other non-delivery applications. The following summarizes the contributions of this paper:

1. Introduce a class of self-aligning mechanisms,

2. Characterize their mechanics and likelihood of misalignment for the 2-blade and 3-blade designs,

3. Formulate an error tolerance metric by which optimal design specifications can be determined, and

4. Verify results in simulation and hardware.

2. PROBLEM SETUP

The mechanism presented in this paper can be viewed independently from any specific application. Thus, our method can be formulated to address a class of self-aligning rotational latches. The generalized problem can be constructed with the following criteria:

- Self-alignment at a fixed position is unique up to a finite number of rotational symmetries,
- Actuation only occurs rotationally about the latch's axis,
- Design parameters should be optimal with respect to any two of the following constraints: space, strength of mating surface material, and error tolerance.

For this paper, the female component with cut engagement slots will be referred to as the *latching pattern* (Fig. 2a), and the male component as the *latch* (Fig. 2b) with equally spaced blades. The scope of this paper only covers self-alignment and deriving optimal designs for the latch and the cut latching pattern geometries. Other areas of interest, such as locking the alignment in place, angle of attack, and load distribution will be considered in future work.

2.1 Assumptions

The majority of our mathematical and geometric derivations rely on a few basic assumptions:

- A counter-clockwise torque is used for latching.
- Slots cut into the latching pattern are radially symmetric pieces of a circle as shown in Fig. 2 with colinear edges extending to R. There is an *island*, the non-hole portion at the center of the design as seen in Fig. 2a, in the center with a separate radius, r.
- The latch face and the surface of the latching pattern are always parallel with one another and interact primarily in a plane, and that out-of-plane effects are minimal. However, this assumption is not strictly required, as shown during the hardware testing in Sec. 5. These tests show that the mechanism could tolerate out-of-plane misalignment, and could still perform successful self-alignment when angled slightly from parallel. Please see the video link in footnote[1].
- The forces applied to the latching mechanism in the X and Y directions during engagement are minimal. This assumption, however, is also not strict as shown during hardware testing where the robotic arm does apply forces in the X and Y directions, see video[1].

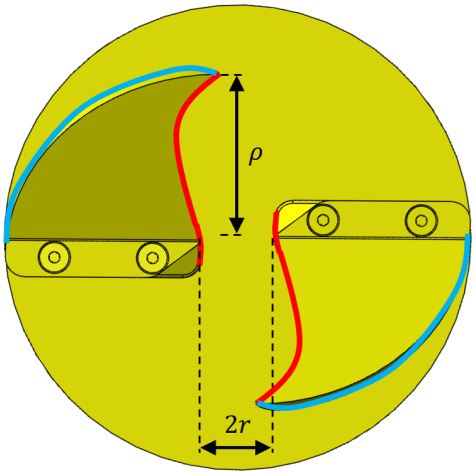

FIGURE 3: TWO BLADE DESIGN SHOWING INNER (RED) AND OUTER (BLUE) EDGES THAT CORRESPOND TO INNER AND OUTER ALIGNMENT METHODS.

Several assumptions on the physical behavior of the latch as the blades interact with the pattern's cut slots. It is assumed that the blades slide along the cardboard pattern's surface and fall into the engagement slots, ultimately resulting in a line of contact between the slot's engagement edge and the blade spacers, shown in red in Fig. 2. Thus, it is also assumed that the shape of the slot itself ultimately does not matter for final engagement, other than the red engagement edges. These edges are radically symmetric with an intersection in the center. Due to this assumption, full cutouts in diagrams are not drawn and are instead treated as a line as seen in Fig. 5,6. This lack of dependence on overall slot shape is verified in practical testing.

In the Sec. 3 derivations, it is assumed that the blade's radial location can be approximated as a single point, depicted by the green dots in Fig. 4,5. In the case of three or more blades, the blade spacer and the engagement edge will only contact at a single point until the latch is fully engaged due to the spacer's rounded shape. Additionally, the width of the spacer can be ignored since the blades have a triangular shape. If the blades are rotated off-center, the sloped surfaces of the blade will contact the pattern edges and force its overall location to adjust until it's aligned with the blade's tip. We tested a mechanism with three pins to verify that this assumption is valid as seen in the supplementary video[1].

In later derivations for Sec. 4, it is assumed that the shape of the blade does not matter beyond the requirements laid out in Sec. 3. For this reason only the point locations of the blade tips and where they start are considered.

In all derivations, the mating pattern surface is assumed to be much stiffer than the forces it is subjected to. This assumption needs verification based on the application and materials involved. In our case, the cardboard's strength is high enough for this assumption to be valid.

Finally, only the 2-blade and 3-blade cases for the latch were considered. Preliminary analyses showed that for more than three

[1] Experiments, verification, and a brief explanation of this paper can be found online at: https://youtu.be/8qShufhR6N0

blades, the error tolerance is worse and there are no additional benefits. For successful alignment, each blade must start its rotation in a separate angular region, since two blades cannot enter the same engagement slot. Since blades must be evenly spaced in 2π rads, increasing the number of blades effectively decreases the angular region available for each blade to start at for successful alignment. Also, a single blade latch is not able to meet the self-aligning requirements as it cannot both constrain the angle and the position of alignment when radially inserted into the mating surface.

3. ALIGNMENT MECHANICS

The next section analyzes the mechanism's sequence of operations and self-aligning motion when the latch is actuated to rotate about its center. For this analysis, it is assumed that the starting configuration for latching is with the blades lightly pressing against the surface of the cut pattern at some initial position (r', θ) and angle of rotation about the latches center axis (γ) similar to the configuration in Fig. 4a.

3.1 Alignment with Two Blades

The two blade latch design consists of blades with an angular separation of π rads as shown in Fig. 3. As the two blades rotate and travel along the surface of the cut pattern, the first blade that contacts with the edge of an engagement slot becomes a new pivot point that the latch begins to rotate about that point.

Once the second blade engages with the colinear edge of the engagement slot, the latch moves along the two aligned edges at the latch's centerline. With only two blades, it would appear impossible to fully constrain the position and rotation, r' and θ, given only a rotational actuation about its center. However, the final constraint needed for a self-correcting motion comes from the blade profiles as the latch inserts its blades further into the the pattern.

This self-correcting motion comes from the contact force between the blade and the engagement edge as it rotates. This contact can occur at the blade's inner edge or outer edge. When the inner edge of the blade presses into the center island of the hole pattern, this is referred to as *inner alignment*, with the inner edge depicted in red in Fig. 3. *Outer alignment* is when the blade edge furthest from the center pushes on the outer edges of the hole during engagement, depicted with the blue edge in Fig. 3. As the latch continues to rotate, self-alignment occurs until the faces of the latch and hole pattern are touching. The latch then becomes fully constrained due to the width of the blade.

3.1.1 Inner Alignment. Since inner alignment uses the inner edge of the blade, the blade needs to taper from its maximum allowable distance from the center, W, at the tip of its blade to r. Let $f(t)$ describe the inner edge contour, with $f(0) = (\rho, \theta)$ and $f(1) = (r, 0)$. As long as this contour follows the property that $||f(t)||$ is monotonically decreasing, then alignment will be successfully achieved.

3.1.2 Outer Alignment. For outer alignment, no center island is needed and the blade uses its outer edge of the hole pattern to align. In this case, the blade tapers out from its minimum distance from the center ρ at the blade's tip to W when fully aligned.

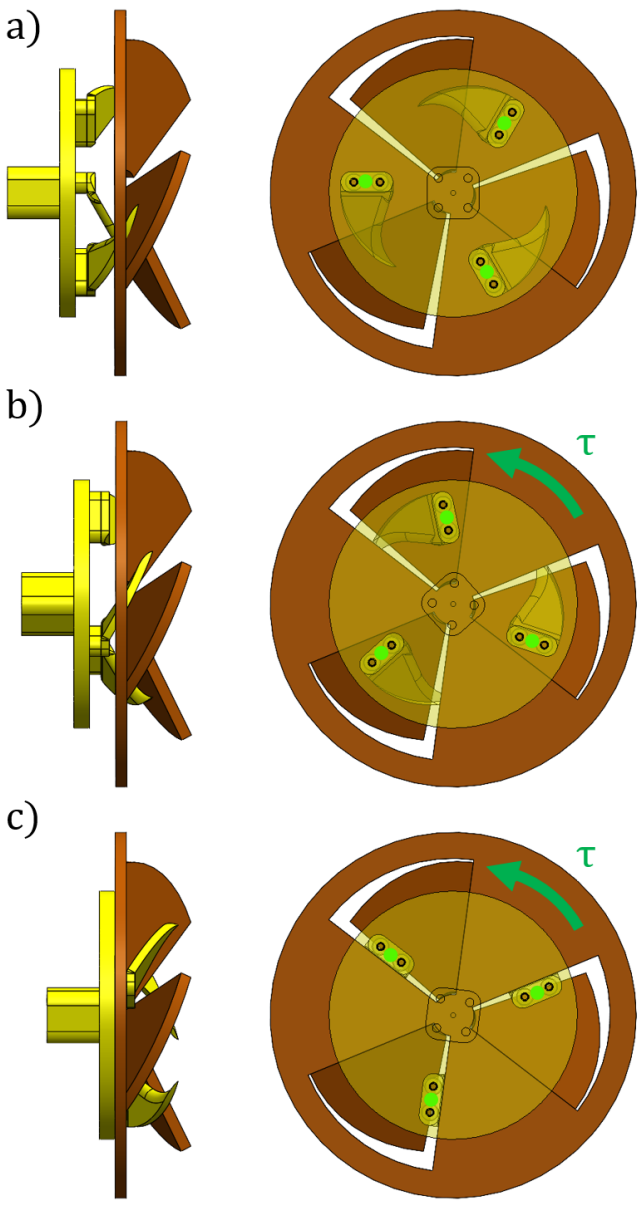

FIGURE 4: SHOWS A SEQUENCE OF A THREE BLADE DESIGN SPINNING TO ALIGN.

This contour has a $f(t)$ where $f(0) = (\rho, \theta)$ and $f(1) = (W, 0)$. If the contour obeys the property that $||f(t)||$ is monotonically increasing, then alignment will succeed.

If a blade is designed to use both inner and outer alignment at the same time, the alignment force will be generated by whichever blade profile is currently in contact with an engagement edge.

3.2 Alignment with Three Blades

The process of aligning with three blades can be broken down into four stages: no blade engaged, then one engaged, followed by two, and then finally all three. Note that it is not required to start at the first stage, although it is the most likely case. The blade locations are modeled as points, shown in green in Fig. 4, 5 and mentioned in Sec. 2.

The behavior of the first two stages closely follow the mechanics for the 2-blade case, where the first blade that contacts the edge of an engagement slot becomes the new pivot point that the latch begins to rotate around. The behavior of this pivot point and the direction of velocity can be explicitly stated using instant centers (IC).

From the starting configuration, the mechanism first spins until one point makes contact with an edge. As torque (τ) is continued to be applied, the resulting forces can be seen in Fig. 5a. The figure further shows that the IC is not fully constrained since there is only one line (dotted grey) perpendicular to hole pattern edge (red line). In other words, the IC would need another grey dotted line that intersects to define a fully constrained point. Assuming $\mu F_N \geq \frac{\tau \sin\theta r'}{\rho^2}$, the far right green dot in Fig. 5a will be a stationary point, making it the IC. The blade assembly (large orange circle) rotates like a wheel around that point until the blade (green dot) contacts with the second edge. Even if slipping occurrs the constraint line (in red) would cause the IC to be on the grey line, which would lead to the second point engaging contact (green dot).

Once two points are in contact, the points are only free to slide along the edge of the cutouts as shown in Fig. 5b. The IC for these two velocities appear in the lower right of the figure by a red dot. The resulting velocity (V) direction is in the direction of the closest edge. This will continue until the third and final blade engages.

Finally, the three points provide three independent constraints, fully defining the latches position and orientation given the axis of rotation and direction of τ. In this state the F_N from the edges are equal and opposite to those caused from τ, so the latching mechanism cannot move and is fully constrained at the target alignment.

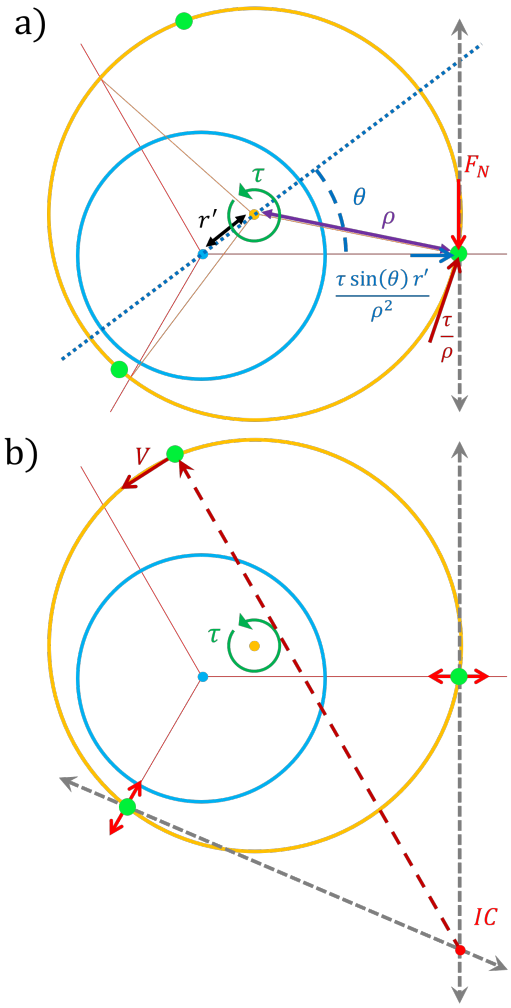

FIGURE 5: VISUAL REPRESENTATION OF THE 3-BLADE (GREEN DOTS ON ORANGE CIRCLE) ALIGNING WITH THE HOLE PATTERN CENTER ISLAND (BLUE CIRCLE). A) FIRST, A SINGLE BLADE ENGAGES THE CUTOUT EDGE (RED) SHOWN BY THE GREEN DOT ON THE FAR RIGHT. B) A SECOND BLADE ENGAGES, RESULTING IN A *V* IN THE DIRECTION OF ALIGNMENT.

4. ALIGNMENT TOLERANCE ANALYSIS

One of the key features of this latching mechanism is its resistance to misalignment. Given an initial position, (x, y) or (r',θ) in polar, and a random orientation, γ, of the blade assembly about its center axis, a probability distribution over the area of the cutout mating surface can be derived.

Under the assumptions stated in Sec. 2, the cut pattern is fully determined by r and R as seen in Fig. 2a. By using optimal values of R^* for a type of alignment and total blade count, we are able to derive the probability distribution function over the entire area of the pattern. In the 2-blade case with inner alignment, setting $R^* \geq 2\rho - r$ is not beneficial as if the center is more than $2\rho - r$ away from the center of the target along the X-axis then the latching will fail. The 3-blade case follows similarly to this and in both cases $R^* = 2\rho - r$. For the 2-blade case with outer align, $R^* \leq W$ in order to align and a larger R increases the potential positions (r', θ) for successful latching. Therefore, $R^*_{out} = W$.

4.1 Two Blades

First, the boundary with zero probability of success, $p = 0$, is established for the 2-blade case. At a minimum, one blade needs to be above the line of engagement and the other below, and the latching will fail if this is not the case. Defining x to be tangent to the colinear engagement edges, the constraint can be given by $|y| \leq \rho$.

Next the inner and outer alignment cases are considered separately. A blade could use both inner and outer alignment at the same time, but the misalignment tolerance would be worse than either a strictly inner or strictly outer alignment. This is because using outer alignment requires $R \leq W$ which is lower than R^* for inner alignment, and inner alignment requires $r > 0$ which makes outer alignment worse. For this reason we only consider the cases separately.

For inner alignment, when one blade contacts the edge and the other rotates around that point and hits the other edge, the two blades' final resting positions must be on opposite sides of the island. This leads to an additional two constraints: $\sqrt{(\rho^2 - y^2)} + (x) \geq r$ and $\sqrt{((\rho)^2 - y^2)} + x \leq (2\rho - r)$. Outer alignment follows a similar behavior, except that the limits are different

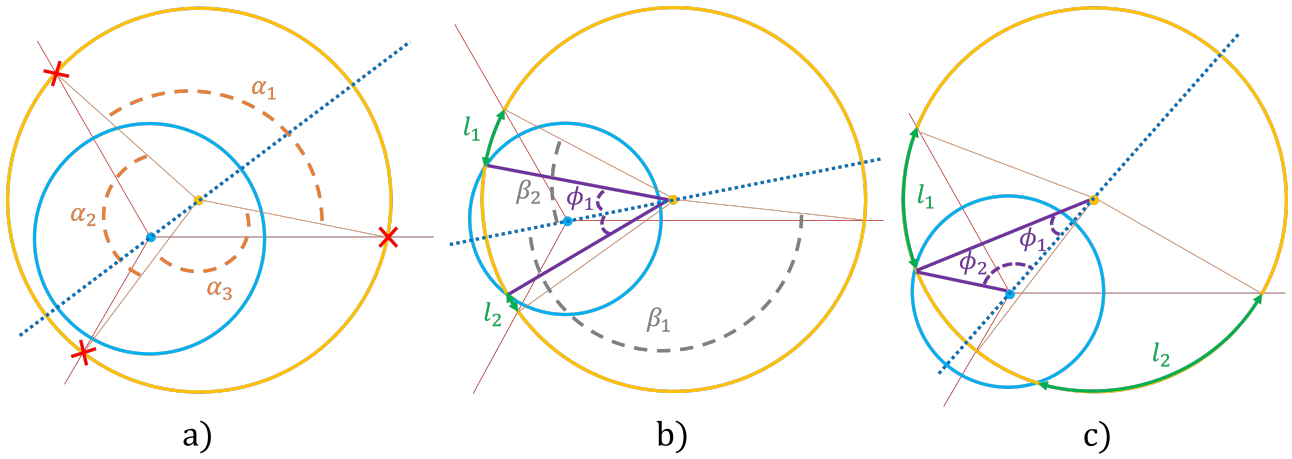

FIGURE 6: THE 3 CASES FOR THE 3-BLADE DESIGN: A) CASE 1 OF ALIGNING WHERE THERE ARE NO INTERSECTIONS, B) CASE 2 OF ALIGNING WHERE BOTH INTERSECTION ARE EITHER COMPLETELY IN α_2 OR α_3, AND C) CASE 3 OF ALIGNING WHERE ONE INTERSECTION IS IN α_2 AND THE OTHER IS IN α_3.

due to using the outer edge of the blade to align and not having a center island. The following are the constraints for the outer alignment: $\sqrt{(\rho^2 - y^2)}+(x) \geq 2\rho - W$ and $\sqrt{((\rho)^2 - y^2)}+x \leq W$. The asymmetry in the inequalities comes from the direction of rotation, and the effect on the pattern can be seen in Fig. 7a. The symmetries in each of these defined regions from the constraints can be rotated by π to complete the probability distribution.

The probability function $p(r', \theta | r, \rho, W)$ for each position is defined over all possible initial angles γ. For simplicity, p is converted to Cartesian coordinates. When doing this and aligning x to be tangential to the colinear engagement edges, p reduces to a function of y:

$$p(x, y | r, \rho, W) = \frac{\pi - 2\tan^{-1}\frac{|y|}{\sqrt{(\rho^2 - y^2)}}}{\pi}$$

This function computes the arc-length of the circle below the engagement edge and divides it by half the total arc-length. The value is divided by two because the angles are only unique up to a rotation of π.

4.2 Three Blades

For the 3-blade case, the blades must be evenly spaced for radial symmetry, so they must be located $\frac{2}{3}\pi$ apart. These probabilities are rotationally symmetric, similar to the boundary equations for the 2-blade case.

In order to achieve successful latching in the 3-blade case, each blade needs to start in separate regions outlined in Fig. 5,6 and not be blocked by the center island. This is because each blade must be able to enter an engagement slot after rotating, and no two blades can physically enter the same slot. If the center of the latch is positioned such that an orientation exists where each blade is located within its own region (and will enter its own slot), then a non-zero probability exists that latching will succeed. If the probability distribution is defined over a single region, it can be rotated by $\frac{2}{3}\pi$ to get the full distribution.

As before, the boundary with zero probability for a single region, i.e., $0 \leq \theta < \frac{2\pi}{3}$, is defined. For latching to be possible, when one blade is engaged and the assembly begins to rotate, the second blade to engage must be able to reach the other side of the island, and so $|r'| \leq \rho$ just as in the 2-blade case.

An additional two constraints appear due to the center island area blocking any blades from entering the engagement slots, which would also result in zero probability, see Fig. 6b, c for how the center island creates new boundary constraints given by: $(y)^2+(x-r)^2 \leq \rho^2$ and $(y - r\sin(\frac{2\pi}{3}))^2+(x - r\cos(\frac{2\pi}{3}))^2 \leq \rho^2$.

The 3-blade probability distribution function is constructed similarly to the function given for the 2-blade design. Deriving a closed form expression, though, is much more complex as there are three cases to be considered:

4.2.1 Case 1. $|r'|$ is sufficiently small so that the trajectory of rotation about the blade assembly's center, shown in orange in Fig. 6a, does not intersect the center island indicated by the blue circle. In this case, the arc length of interest is the smaller of α_2 and α_3, since it defines the first blade to violate a boundary. However, there are also blades located $\frac{2}{3}\pi$ away in the other regions. The feasible arc lengths of these blades need to be considered as well. The minimum of this is divided by $\frac{2}{3}\pi$ to give the probability.

4.2.2 Case 2. The trajectory when rotating about the assembly's center intersects the center island exactly twice as seen in Fig. 6b, c. Depending on where the intersection occurs, the $p(\cdot)$ varies. If the intersections are both in the same region, then it would look similar to Fig. 6b. In this scenario, the arc lengths of l_1 and l_2 are of interest, as well as how much of the other region is available for the blade tip which is $\frac{2}{3}\pi$ away to engage with. This is done for both l_1 and l_2, always taking the minimum of it and its offset. Once this is done all of the resulting arc lengths are summed and divided by $\frac{2}{3}\pi$ to give the probability.

4.2.3 Case 3. The intersections are split across sectors as shown in Fig. 6c. This case is similar to Case 1 where there are no intersections. The only exception is when α_2 and α_3 are blocked by the center island.

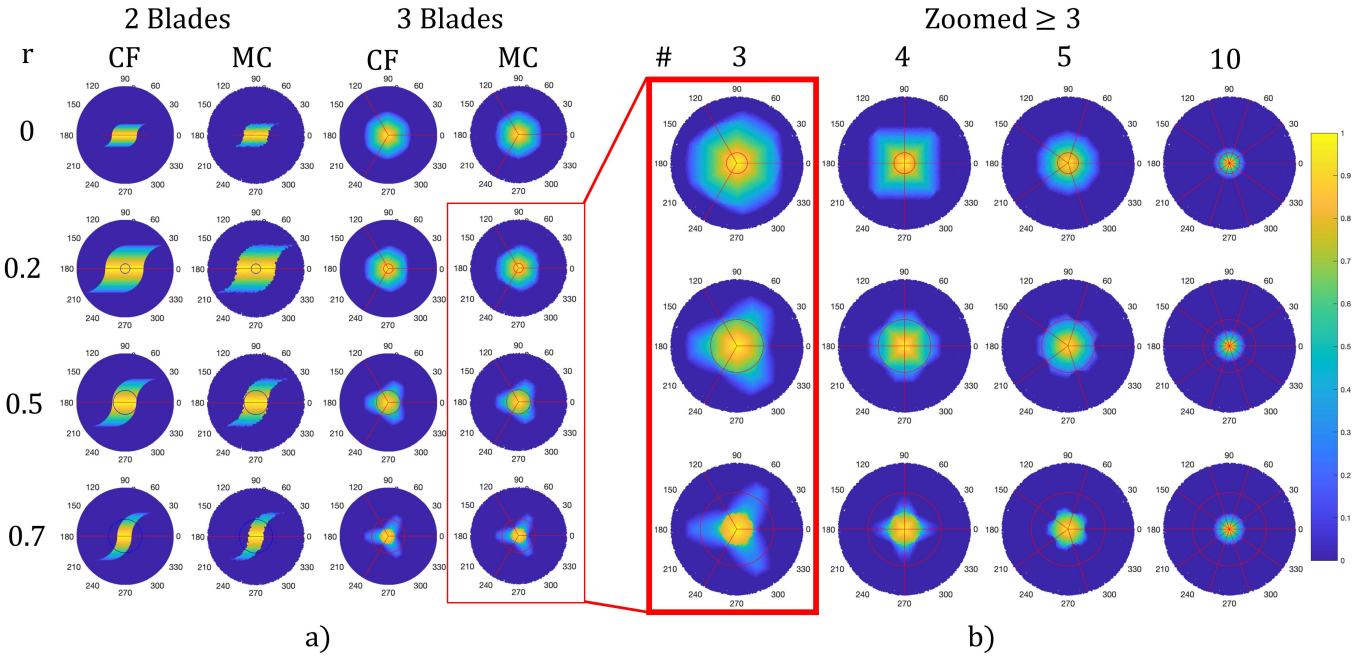

FIGURE 7: DEPICTS p WHERE BRIGHTER COLORS REPRESENT HIGHER PROBABILITIES OF SUCCESS: A) MONTY CARLO (MC) EXPERIMENTS AND CLOSED-FORM (CF) EXPRESSIONS FOR BOTH THE 2 AND 3-BLADE DESIGN, WITH r VALUES OF 0, 0.2, 0.5 AND 0.7. FOR THE 2-BLADE CASE, ALL RESULTS ARE FOR INNER ALIGNMENT EXCEPT FOR WHEN R=0 WHICH IS FOR OUTER. B) ZOOMED IN FIGURES OF OUR MC EXPERIMENTS FOR 4, 5 AND 10 BLADES WITH R VALUES OF 0.2, 0.5 AND 0.7, WHERE THE 3-BLADE CASE WAS ADDED TO SHOW HOW INCREASING THE NUMBER OF BLADES DECREASES THE MISALIGNMENT TOLERANCE. SEE THE APPENDIX FOR HIGHER RESOLUTION IMAGES OF CF DISTRIBUTIONS.

The probability function for the 3-blade case is not continuous since it must take into account different cases and take minimum values. In order to present the closed form expression of p, several intermediate variables are provided to simplify the expression (also depicted in Fig. 6):

$$\beta_1 = \frac{\pi}{3} - sin^{-1}(\frac{r' \sin(\theta)}{\rho}) - \theta$$

$$\beta_2 = \frac{\pi}{3} - \sin^{-1}(\frac{r'}{\rho \sin(2\pi/3 - \theta)}) + \theta$$

$$\beta_3 = \frac{\pi}{3} - sin^{-1}(\frac{r' \sin(\frac{2\pi}{3} + \theta)}{\rho}) - \theta$$

$$\alpha_1 = (2\pi - (\beta_2 + \beta_1))$$

$$\alpha_2 = \beta_3 + \beta_2$$

For 3 blades p is as follows:

1. Case 1: $r' \leq \rho - r$ (0 or 1 intersections with the island)
   $p = \min(\alpha_2 + \alpha_3 - 2\pi/3, \min(\alpha_2, \alpha_3))$
2. Case 2: $r' > \rho - r$ (2 intersections with the island)
   (a) $\theta - \phi_2 < 4\pi/3$ (2 intersections in α_2)
   $l_1 = \beta_2 - \phi_1$
   $l_2 = \beta_1 - \alpha_3 - \phi_1$
   $p_1 = \min(\max(\alpha_2 + \alpha_3 - 2\pi/3, 0), l_1)$
   $p_2 = \min(\max(\alpha_2 + \alpha_3 - l_1 - 2\phi_1 - 2\pi/3, 0), l_2)$
   $p = p_1 + p_2$
   (b) $\theta + \phi_2 > 4\pi/3$ (2 intersections in α_3)
   $p_1 = \min(\max(\alpha_2 + \alpha_3 - 2\pi/3, 0), l_1)$
   $p_2 = \min(\max(\alpha_2 + \alpha_3 - 2\pi/3 - l_1 - 2\phi_1, 0), l_2)$
   $p = p_1 + p_2$
3. Case 3: $r' > \rho - r$ (1 intersection in α_2 & other in α_3)
   $\theta + \phi_2 \leq 4\pi/3$ and $\theta - \phi_2 \geq 4\pi/3$
   $p_1 = \max(\min(l_1, l_2) + 2\phi_1 - 2\pi/3, 0)$
   $p_2 = \min(\alpha_2 + \alpha_3 - 2\pi/3, \min(l_1, l_2))$
   $p = \max(p_2 - p_1, 0)$

4.3 Alignment Tolerance Metric Ψ

With probability p now defined, the performance of different latch designs can be compared based on their alignment tolerance. Ψ is a scalar quantity that can help compare relative designs by summing over p:

$$\Psi(W, \rho, r) = \int_{D(0, W*c)} p(r', \theta | r, \rho, W) dA \quad (1)$$

where $p(r', \theta | r, \rho, W)$ is defined above, and c is a constant based on the application. It is constrained to $c \leq \sqrt{(5)}$ as this will capture the entire distribution. Due to the complexity and piecewise nature of p, Ψ can most easily be computed numerically. Ψ is not unitless to allow it to maintain a physical meaning for design comparisons. Comparisons are made on a relative scale for similar designs, but there are nuanced specifications in which looking at both p and Ψ could be even more beneficial.

Although these equations are valid for all $\rho \leq W$, there is an optimal value of ρ which only depends on whether the alignment case is an inner or outer alignment. If it is inner alignment, the optimal is: $\rho^*_{in} = W$. This is due to $\Psi(W, \rho, r) \leq \Psi(W, W, r)$, since $p(r', \theta | r, \rho, W) \leq p(r', \theta | r = W, \rho = W)$. This is less obvious for the outer alignment case, as increasing ρ increases one bound while decreasing the other. Because of this, it is necessary to compute the optimal value by a numerical method resulting in: $\rho^*_{out} \approx 0.48W$.

The best case offset from the center comes from the 2-blade case using inner alignment in the upper left most corner when r approaches 0 as seen in Fig. 10f. The coordinates of that point are $(2\rho - r, \rho)$. When r goes to 0, it becomes $\sqrt{5}\rho^*_{in}$. Although r can never truly equal zero in a practical design, it can be reduced to nearly zero if the latching pattern incorporates a stronger material such as metal or plastic to reinforce the center island.

4.4 Monte Carlo vs Theoretical

Our derivations are validated by comparing Monte Carlo simulations (MC) to our closed-form expressions (CF) as shown in Fig. 7. The left image, Fig. 7a, shows the two probability density functions side by side for comparison. The two are the nearly identical, verifying our CF results.

Inspecting Fig. 7a indicates that the 2-blade design has a larger overall area of feasible positions and a larger area with a high probability of success, depicted by brighter colors. Fig. 7b shows a zoomed-in view of the bottom 3-blade patterns from Fig. 7a and increases the number of blades in the pattern. It can clearly be seen that the more number of blades in the pattern, the less robust it is for handling misalignment. Higher resolution images are provided in the Appendix for closer inspection.

5. DESIGN CASE STUDY

5.1 Design Framework

Using Ψ defined in (1), three different design methods can be outlined based on known constraints for a particular application. These can be alignment tolerance Ψ^*, a minimal r based on material properties, or a maximum W based on the size constraints for the latching mechanism.

The designer must first decide if 2 or 3 blades work better for the application. The 2-blade design has a better Ψ but uses r to align, while 3 blades has a worse Ψ but does not use r for alignment. The flow charts shown in Fig. 8 show the design process for picking the best design given two of the three parameters. If it is for the 3-blade design, then only the inner alignment parts are applicable. This comes from the fact that R^* and ρ^* are the same for both 2-blade inner alignment and 3-blade alignment.

Using Fig. 8a, a viable design for both 2-blade and 3-blade mechanisms for use on LIMMS was developed. We first conducted experiments and determined $r \geq 8mm$ based on the strength of cardboard. Since corrugated cardboard is an orthotropic composite material, patterns were cut with the flutes oriented the same way to eliminate effects from the material anisotropic properties [9]. In addition, since the latch must be able to fit on the existing LIMMS end effector: $W = 35mm$.

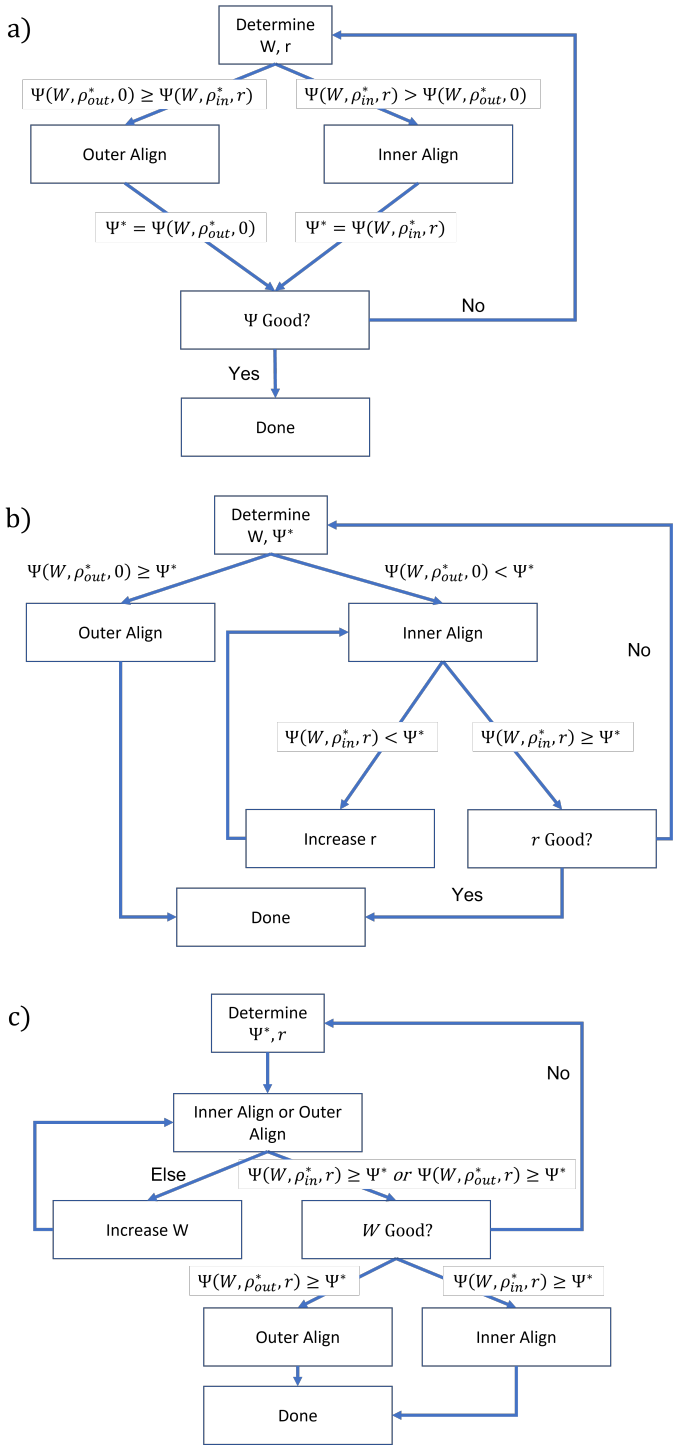

FIGURE 8: DESIGN PROCESS DERIVED FOR 3 SEPARATE DESIRED DESIGN SPECIFICATIONS USING DEFINED METRIC Ψ. THE PROCESS IS SPLIT BASED ON STARTING PARAMETERS: A) *W* AND *r*, B) *W* AND Ψ*, AND C) Ψ* AND *r*

For the 2-blade design, given our constraints for W and r: $\Psi(35, \rho^*_{out}, 0) = 0.0310$ and $\Psi(35, \rho^*_{in}, 8) = 0.0957$. Based on this, the more optimal design is with inner alignment where $\rho = \rho^*_{in} = 35mm$, which gave a $\Psi = 0.0957$. The process for the 3-blade design followed similarly, since given our W and r,

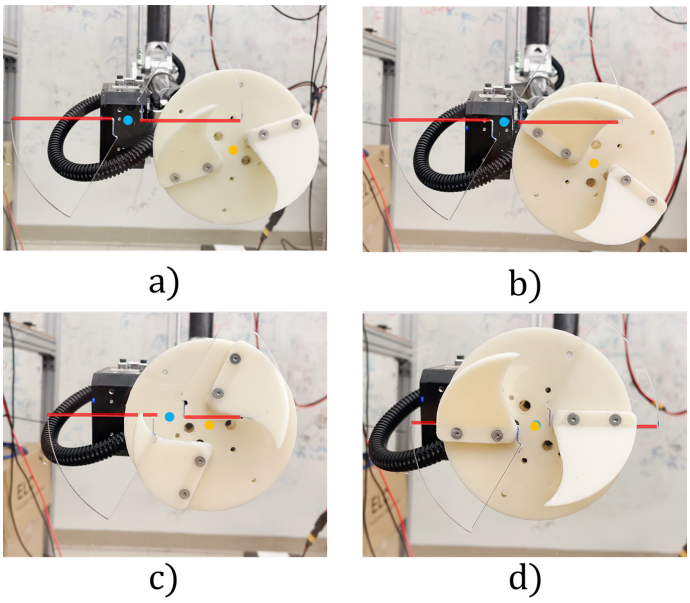

FIGURE 9: DEPICTS 2-BLADE LATCHING WITH AN ACRYLIC MATING SURFACE.

only inner alignment is applicable. In this case $\Psi(35, \rho^*_{in}, 8) = 0.0593$.

5.2 Verification Experiments

To verify the results of our design methodology, both the 2-blade and 3-blade mechanisms were tested using two different mating surfaces. The first surface tested was cardboard, required for the last mile delivery problem. The cardboard chosen for experiments was C-flute cardboard with a thickness of 4.4 mm, chosen to best simulate the average properties of common shipping boxes. The second surface was acrylic, which is transparent and has a lower coefficient of friction. This was to explore the option of integrating a plastic insert with the cardboard pattern for reinforcement and to study the mechanical behavior of the latch as it rotates.

The blade mechanisms were attached to YORI, a five degree of freedom (DoF) robotic arm [10], to simulate the mechanism's behavior when attached to the LIMMS platform. YORI was operated using simple PID (proportional-integral-derivative) controllers, with minimal gain tuning. In these tests, the latching mechanisms were able to align and hold as expected (as shown in video[1]). Note that the base used for this prototype was larger than $W = 35mm$ in order to to accommodate multiple testing setups as seen in Fig. 9. The blades, however, are optimal for a W of 35 mm.

6. CONCLUSION

In this paper, we analyzed a class of self-aligning rotational latching mechanisms and manufactured prototypes for use on LIMMS. The probability distributions for both 2-blade and 3-blade designs were formally derived and verified using MC and CF. By inspection of Fig. 7, it is clear that the 2-blade design outperforms the others in terms of self-alignment. As the numbers of blades increased, the rate of success decreased overall. From the probability distribution, a new metric Ψ was introduced to compare relative designs and quantify alignment tolerance. This metric also demonstrated that the 2-blade latching mechanism achieves self-alignment more consistently than the other designs. Depending on the specific application, using both Ψ and the probability distribution may be preferable when designing the latch as there may be subtle trade-offs between robustness in (x, y) and θ. Our analysis also showed that the 2-blade design can be as far as $\sqrt{5}\rho^*_{in}$ away and still align successfully with the cut latching pattern.

Our analyses were formalized as a design process for this type of latching mechanism to find optimal design specifications for specific constraints as laid out in Fig. 8. We then used this methodology to manufacture both a 2-blade and 3-blade latching mechanism. The theory was then tested using these mechanisms with a robotic arm holding a single off-center position with PID control. The results of these experiments with two different surface materials were consistent with our theory.

6.1 Future Work

The first topic to explore would be the development of a generalized p function for n blades. Additionally, it would be useful to derive a model for optimal blade angle based on certain material properties to determine the best geometries for latching strength. Since the latching strength will be a function of pattern geometry, mechanism fabrication, and the orthotropic material properties of cardboard, these topics will be studied more in depth for future designs to best optimize latching performance and rigidity. Finally, methods for locking the rotation after torque is no longer being applied will be explored. The latching pattern itself provides geometry that constrains 5 out of the 6 DoFs, where the last degree of freedom (axial rotation) must be fully constrained to form a rigid connection. There are currently two options being explored. One way to constrain rotation is to use an additional hole pattern with pins that push in to prevent the blades from rotating out of the pattern. Another method would be to have the blades pull in towards the base of the mechanism after alignment, which would compress the cardboard, restrict backwards rotation, and increase overall rigidity. With these improvements, this mechanically intelligent latching mechanism could allow LIMMS to perform its operations smoothly and reliably.

ACKNOWLEDGEMENTS

The authors would like to thank LG Electronics for sponsoring this research and giving useful feedback.

REFERENCES

[1] Zhu, T, Fernandez, GI, Togashi, C, Liu, Y and Hong, DW. "Feasibility Study of LIMMS, A Multi-Agent Modular Robotic Delivery System with Various Locomotion and Manipulation Modes." *2022 19th International Conference on Ubiquitous Robots (UR)*. 2022. IEEE.

[2] Gökler, Mustafa Ilhan and Koc, Murat Bilgin. "Design of an automatic tool changer with disc magazine for a CNC horizontal machining center." *International Journal of Machine Tools and Manufacture* Vol. 37 No. 3 (1997): pp. 277–286.

[3] Hays, Anthony B, Tchoryk Jr, Peter, Pavlich, Jane C, Ritter, Greg A and Wassick, Gregory J. "Advancements in design of an autonomous satellite docking system." *Spacecraft Platforms and Infrastructure*, Vol. 5419: pp. 107–118. 2004. SPIE.

[4] Sproewitz, Alexander, Billard, Aude, Dillenbourg, Pierre and Ijspeert, Auke Jan. "Roombots-mechanical design of self-reconfiguring modular robots for adaptive furniture." *2009 IEEE international conference on robotics and automation*: pp. 4259–4264. 2009. IEEE.

[5] Parrott, Christopher, Dodd, Tony J. and Groß, Roderich. "HiGen: A high-speed genderless mechanical connection mechanism with single-sided disconnect for self-reconfigurable modular robots." *2014 IEEE/RSJ International Conference on Intelligent Robots and Systems*: pp. 3926–3932. 2014. DOI 10.1109/IROS.2014.6943114.

[6] Sproewitz, Alexander, Asadpour, Masoud, Bourquin, Yvan and Ijspeert, Auke Jan. "An active connection mechanism for modular self-reconfigurable robotic systems based on physical latching." *2008 IEEE International Conference on Robotics and Automation*: pp. 3508–3513. 2008. IEEE.

[7] Cruijssen, HJ, Ellenbroek, M, Henderson, M, Petersen, H, Verzijden, P and Visser, M. "The European robotic arm: A high-performance mechanism finally on its way to space." *42nd Aerospace Mechanisms Symposium*. 2014.

[8] Yip, Hiu Man, Wang, Zerui, Navarro-Alarcon, David, Li, Peng, Liu, Yun-hui and Cheung, Tak Hong. "A new robotic uterine positioner for laparoscopic hysterectomy with passive safety mechanisms: Design and experiments." *2015 IEEE/RSJ International Conference on Intelligent Robots and Systems (IROS)*: pp. 3188–3194. 2015. IEEE.

[9] Aboura, Zoheir, Talbi, Nabil, Allaoui, Samir and Benzeggagh, ML. "Elastic behavior of corrugated cardboard: experiments and modeling." *Composite structures* Vol. 63 No. 1 (2004): pp. 53–62.

[10] Noh, Donghun, Liu, Yeting, Rafeedi, Fadi, Nam, Hyunwoo, Gillespie, Kyle, Yi, June-sup, Zhu, Taoyuanmin, Xu, Qing and Hong, Dennis. "Minimal Degree of Freedom Dual-Arm Manipulation Platform with Coupling Body Joint for Diverse Cooking Tasks." *2020 17th International Conference on Ubiquitous Robots (UR)*: pp. 225–232. 2020. DOI 10.1109/UR49135.2020.9144811.

[11] Garbowski, Tomasz, Gajewski, Tomasz and Grabski, Jakub Krzysztof. "Estimation of the compressive strength of corrugated cardboard boxes with various openings." *Energies* Vol. 14 No. 1 (2021): p. 155.

[12] Garbowski, Tomasz, Knitter-Piątkowska, Anna and Mrówczyński, Damian. "Numerical homogenization of multi-layered corrugated cardboard with creasing or perforation." *Materials* Vol. 14 No. 14 (2021): p. 3786.

[13] Garbowski, Tomasz, Gajewski, Tomasz and Grabski, Jakub Krzysztof. "The role of buckling in the estimation of compressive strength of corrugated cardboard boxes." *Materials* Vol. 13 No. 20 (2020): p. 4578.

[14] Gallo, Javier, Cortés, Fernando, Alberdi, Elisabete and Goti, Aitor. "Mechanical behavior modeling of containers and octabins made of corrugated cardboard subjected to vertical stacking loads." *Materials* Vol. 14 No. 9 (2021): p. 2392.

APPENDIX A. CF PROBABILITY DISTRIBUTIONS

Several interesting higher resolution CF probability distribution functions are shown in this section for 2 and 3 blade designs on the next page. In the three blade designs, there are subtle details, and there does not seem to be one consistent pattern as the island (red circle) scales. The red lines in the figure show the separation of regions that indicate symmetry.

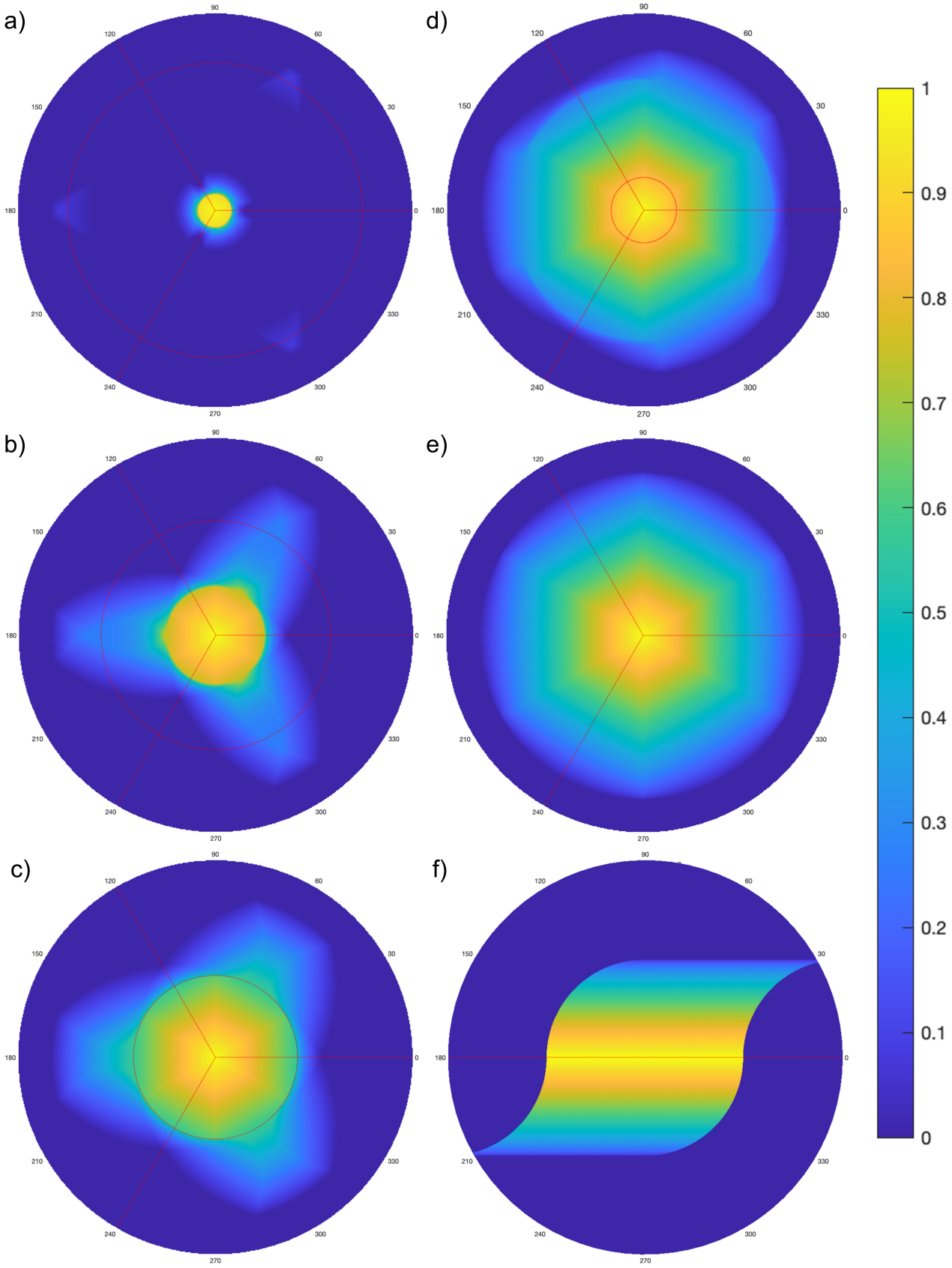

FIGURE 10: PROBABILITY DISTRIBUTION FUNCTIONS: A) 3-BLADE R=0.9, B) 3-BLADE R=0.7, C) 3-BLADE R=0.5, D) 3-BLADE R=0.2, E) 3-BLADE R=0, AND F) 2-BLADE $r \rightarrow 0$ FOR AN INNER ALIGNMENT.